NASA/TM—1998-206639/REV1

Analysis of a Rocket Based Combined Cycle Engine During Rocket Only Operation

T.D. Smith and C.J. Steffen, Jr.
Lewis Research Center, Cleveland, Ohio

S. Yungster
Institute for Computational Mechanics in Propulsion, Cleveland, Ohio

D.J. Keller
RealWorld Quality Systems, Inc., Cleveland, Ohio

National Aeronautics and
Space Administration

Lewis Research Center

October 1998

Trade names or manufacturers' names are used in this report for identification only. This usage does not constitute an official endorsement, either expressed or implied, by the National Aeronautics and Space Administration.

Available from

NASA Center for Aerospace Information
7121 Standard Drive
Hanover, MD 21076
Price Code: A03

National Technical Information Service
5287 Port Royal Road
Springfield, VA 22100
Price Code: A03

ANALYSIS OF A ROCKET BASED COMBINED CYCLE ENGINE DURING ROCKET ONLY OPERATION

T.D. Smith and C.J. Steffen, Jr.
National Aeronautics and Space Administration
Lewis Research Center
Cleveland, Ohio 44135

S. Yungster
Institute for Computational Mechanics in Propulsion (ICOMP)
Cleveland, Ohio 44135

and

D.J. Keller
RealWorld Quality Systems, Inc.
Cleveland, Ohio 44116

ABSTRACT

The all rocket mode of operation is a critical factor in the overall performance of a rocket based combined cycle (RBCC) vehicle. However, outside of performing experiments or a full three dimensional analysis, there are no first order parametric models to estimate performance. As a result, an axisymmetric RBCC engine was used to analytically determine specific impulse efficiency values based upon both full flow and gas generator configurations. Design of experiments methodology was used to construct a test matrix and statistical regression analysis was used to build parametric models. The main parameters investigated in this study were: rocket chamber pressure, rocket exit area ratio, percent of injected secondary flow, mixer-ejector inlet area, mixer-ejector area ratio, and mixer-ejector length-to-inlet diameter ratio. A perfect gas computational fluid dynamics analysis was performed to obtain values of vacuum specific impulse. Statistical regression analysis was performed based on both full flow and gas generator engine cycles. Results were also found to be dependent upon the engine cycle assumptions. The statistical regression analysis determined that there were five significant linear effects, six interactions, and one second-order effect. Two parametric models were created to provide performance assessments of an RBCC engine in the all rocket mode of operation.

INTRODUCTION

For years rocket-based combined cycle (RBCC) engine systems have been envisioned as the means to achieve affordable single-stage-to-orbit (SSTO).[1-7] The inherent advantage of RBCC engine systems is the increased specific impulse, or fuel efficiency, of the airbreathing system as compared to an all rocket SSTO vehicle. A more fuel efficient engine system will increase the vehicle payload mass fraction and thus reduce the cost per pound to orbit. A typical RBCC engine will operate in four modes; (1) ejector ramjet, (2) ramjet, (3) scramjet, and (4) all-rocket. In general, the performance of the rocket is based on the design chamber pressure, mixture ratio, propellants, and exit area ratio of the engine. However, for most RBCC systems the rocket is simply a subset of the engine. While a significant amount of analysis has been performed on modes 1 to 3, little analysis has been performed on mode 4. However, as shown in Ref. 8, the performance of an RBCC system in mode 4 can have a significant affect on total system performance. Depending upon the assumed trajectory, the mode 4 performance can have a nearly 1:1 relationship with overall system performance. Therefore, having an accurate assessment of the rocket mode performance is critical and may influence engine design and layout.

Rockets are generally used in two of the modes of operation, ejector ramjet and all-rocket for orbit insertion. To accomplish the ejector pumping in mode 1, the rockets are generally located in the forward section of the engine (Fig. 1(a)) followed by a mixer-ejector section. This section can be round, square, straight, or diverging with a single rocket or multiple rockets. The addition of the mixer-ejector section is required for mode 1 performance, however, this configuration is not ideal for the all-rocket mode 4 performance. Because of the open area required for the inlet air, there is a free expansion of the rocket plume to the mixer-ejector wall. Once the plume impinges onto the walls it can create a series of reflected shocks inside of the engine. As a result, the flow path is significantly different from an optimum rocket nozzle with the same overall expansion area ratio. Over the years a significant amount of work has

been performed on developing methods for designing optimal rocket nozzles, Fig. 1(b).[9,10] However, there is a lack of design or analysis for an RBCC system operating in a mode 4 configuration.

The objective of the present study is to quantify the effects of the mixer-ejector section on the all-rocket mode performance. A Navier-Stokes, perfect gas computational fluid dynamics (CFD) analysis was performed with the NPARC[11] computer code. An axisymmetric model, which consisted of a single rocket engine with a variable duct, was chosen for ease of modeling. The main parameters investigated in the study were: chamber pressure, rocket exit area ratio, percent of injected secondary flow, mixer-ejector inlet area ratio, mixer-ejector area ratio, and mixer-ejector length-to-inlet diameter ratio. The CFD calculations were used to assess the specific impulse efficiencies of the various RBCC configurations studied. Specific impulse efficiencies were calculated based on both full flow and gas generator system assumptions. Design of experiments (DOE) was used to set up the test matrix and statistical regression models were created based upon the CFD results. The statistical models account for interactions and curvilinear effects between the six parameters.

SYMBOLS

A^*	rocket throat area ($in.^2$)
A_3	mixer-ejector inlet area ($in.^2$)
A_6	mixer-ejector exit area ($in.^2$)
D_3	mixer-ejector inlet diameter (in.)
E	statistical model error term (percent)
FF	results from full-flow analysis
F	thrust (lb_f)
g_o	gravitational constant (32.174 lb_m-ft/lb_f sec^2)
GG	results from gas-generator analysis
Isp	specific impulse (sec)
Isp_{CFD}	specific impulse from CFD results (sec)
$Isp_{isentropic}$	specific impulse from isentropic calculations (sec)
L	mixer-ejector length (in.)
$\dot{m}_p$	primary rocket mass flow (lb_m/sec)
$\dot{m}_s$	injected secondary flow (lb_m/sec)
m_s	percent injected secondary flow, $\left(\frac{\dot{m}_s}{\dot{m}_p} \times 100\right)$
$\dot{m}_t$	total mass flow (lb_m/sec)
N	number of data points used in the multiple linear regression
P	number of terms in the final statistical model
Pc	rocket engine chamber pressure (psia)
p_6	mixer-ejector exit static pressure ($lb_f/in.^2$)
Q	dynamic pressure (lb_f/ft^2)
R^2	residual error term
$S_{Y.X}$	goodness of fit statistic between experimental value and model prediction
t	multiplicative statistical constant dependent upon N-P
u_6	mixer-ejector axial exit velocity (ft/sec)
x_i	statistical model independent variable
x_{imin}	statistical model independent variable–minimum value possible
x_{imax}	statistical model independent variable–maximum value possible
X_i	statistical model input transformed variable
Y_i	calculated Isp for statistical model.
$\overline{Y}$	mean calculated Isp for statistical model
$\hat{Y}_i$	predicted value of the output variable from statistical model
β	statistical model coefficient
ε_{ME}	mixer-ejector nozzle exit area ratio
ε_R	rocket exit area ratio
γ	ratio of specific heats
η_{Isp}	specific impulse efficiency (percent)
ρ	density (lb_m/ft^3)

RBCC ENGINE CONFIGURATION

An axisymmetric engine geometry was used for this analysis (Fig. 1(a)). The system consists of a single rocket engine in the forward section of a mixer-ejector duct. The Rao nozzle design code[12] was used to design the nozzle contour for each rocket exit area ratio. The rocket chamber conditions assumed a gaseous oxygen and gaseous hydrogen system at a mixture ratio of 6. The main RBCC engine parameters investigated in this study were:

The mixer-ejector inlet area (A_3/A^*) is a ratio of the total area at the beginning of the mixer-ejector to the rocket throat area. Total mixer-ejector exit area ratio (A_6/A^*) is the total available for expansion. The mixer-ejector area ratio is the amount of expansion provided by the mixer-ejector only (A_6/A_3). Percentage of injected secondary flow (m_s) is the ratio of injected secondary flow to primary rocket flow.

DATA ANALYSIS

The measure of performance used in this analysis is specific impulse efficiency. To calculate specific impulse, the CFD results were used to calculate mass flow and thrust with a trapezoidal integration across the mixer-ejector exit plane, Eqs. (1) and (2) respectively. In this analysis, ambient pressure outside the nozzle was set at vacuum conditions. As a result, the effect of ambient pressure on thrust is negligible. The values were then used to calculate the specific impulse, Eq. 3:

$$\dot{m}_t = \int_{exit} (\rho u_6) dA_6 \tag{1}$$

$$F = \int_{exit} \left(\rho u_6^2 + p_6\right) dA_6 \tag{2}$$

$$Isp_{CFD} = \frac{F}{\dot{m}_t} \tag{3}$$

The calculated Isp results from the CFD analysis were compared to the Isp values from isentropic flow calculations which represent the theoretical ideal performance levels.

$$\eta_{Isp} = \frac{Isp_{CFD}}{Isp_{Isentropic}} \tag{4}$$

Combustion efficiency is assumed to be 100 percent for all cases. Ideal performance is based on expanding the flow to the maximum area ratio available at the mixer-ejector exit.

Due to the presence of injected secondary flow, there are two methods to calculate the ideal performance. Each is based upon different system cycle assumptions. The first method is to base the ideal performance (Isp_{FF}) on the rocket flow only ($\dot{m}_p = \dot{m}_t$), a full-flow cycle. Specific impulse is thus:

$$Isp_{FF} = \frac{F}{\dot{m}_p} \tag{5}$$

In a full-flow system all of the propellants available are routed to the engine where they are mixed and burned. Any flow not consumed by the rocket is considered a loss. In this analysis the secondary bleed flow ($\dot{m}_s$) is a loss. The second method is a comparison to a gas generator type of system (Isp_{GG}) and is shown in Eq. (6).

$$Isp_{GG} = \frac{F}{\dot{m}_p + \dot{m}_s} \tag{6}$$

In a typical gas generator cycle, more propellant is required to power the turbomachinery than is used in the rocket combustion chamber. The excess propellants are then vented overboard with a minimal contribution to thrust. In an RBCC vehicle, the possibility also exists that additional propellants would be carried on-board for cooling of vehicle surfaces. However, in this system the secondary flow is being routed back into the engine flow path in an attempt to make the engine more efficient by increasing base pressure.

DESIGN OF EXPERIMENTS STRATEGY

The DOE analysis matrix was developed to reduce the number of tests required and to develop a parametric performance model. To fully model all curvilinear effects and potential interactions a total of 729 (i.e. 3^6) cases would have been required. Using DOE, the full matrix was reduced to a total of 36 cases; enough to examine the curvilinear effects and interactions. The 36 case model was further reduced to nine experiments to examine only the linear effects. Results from the linear screening analysis can be found in Ref. 8. Table II lists the detailed configuration for each of the thirty-six cases in the model along with the total area ratio as a reference. The result is a response surface model (RSM) analysis that was obtained using Isp efficiencies to determine the effect each variable had on performance.

All RSM analyses were conducted using the RS/CLIENT™ statistical software. Two sets of statistics are reported for each data set, the estimated coefficients and the confidence level for these values. The confidence levels are the estimated probabilities that the coefficients are different from zero. Any coefficient having a confidence level less than 90 percent was considered insignificant and its corresponding term dropped from the model. Values with confidence levels less than 95 percent are considered weak effects upon the model.

In a typical regression analysis, significance is identified and quantified relative to an estimate of system noise based on a number of repeated experiments. However, a computer code should generate no noise and repeating each case should generate the same answer. For both the RSM analyses, the noise terms were generated with the residual variation from fitting 36 data points with a 14-term model.

For each data set a simple relationship was based on the input variables. Each variable has an associated coefficient.

$$\eta_{Isp} = \beta_0 + \beta_1 X_1 + \beta_2 X_2 \ldots + \beta_7 X_1 X_2 \ldots + \beta_{27} X_6^2 \tag{7}$$

For the current analysis the variables were normalized to values of ±1 so that the estimated coefficients would reflect the relative strengths of the effects. Hence, the larger a coefficient value, the greater its influence on the final result. As a result, the transformed X_i variable is actually:

$$X_i = \frac{x_i - \left(\frac{x_{i\,max} + x_{i\,min}}{2} \right)}{\frac{x_{i\,max} - x_{i\,min}}{2}} = \frac{x_i - \text{midpoint}}{\frac{\text{range}}{2}} \tag{8}$$

Also calculated are the values for residual (R^2), goodness of fit ($S_{Y.X}$), and an error estimate (E). The $S_{Y.X}$ is a goodness of fit statistic which summarizes the agreement between the actual output value and the associated model predictions.

$$R^2 = \frac{\sum\left(\hat{Y}_i - \overline{Y}\right)^2}{\sum\left(Y_i - \overline{Y}\right)^2} \tag{9}$$

$$S_{Y.X} = \sqrt{\frac{\sum\left(Y_i - \hat{Y}_i\right)^2}{(N-P)}} \tag{10}$$

$S_{Y.X}$ may be used to calculate approximate prediction errors (E) as follows.

$$E \approx t \times S_{Y.X} \tag{11}$$

where t is a multiplicative constant that changes depending on the residual degrees of freedom (N-P). These t constants can be located in any statistical test or mathematical handbook[13] under student's t-test. This is the variation in each data value derived from the model for Isp efficiency.

CFD ANALYSIS

The flow solver chosen for this study was NPARC v3.0 which is a multidimensional flow simulator used for a wide variety of fluid flow analyses within the aerospace community. NPARC is a finite difference code for structured, multiblock grids, and is bound by the assumption of the perfect gas law. The cases discussed here assumed steady, axisymmetric, turbulent flow through the RBCC engine. Turbulence was modeled with the Spalart-Allmaras (SA)1-equation turbulence model.[14] A more detailed discussion of the CFD modeling can be found in Ref. 15.

The physical boundaries of the RBCC engine have been modeled as standard adiabatic, no-slip surfaces. The combustion chamber was simulated by specifying the constant total conditions given in Table III. The total conditions were obtained by running a one-dimensional chemical equilibrium code[16] for a given chamber pressure, with ambient temperature gaseous hydrogen and gaseous oxygen as propellants at a mixture ratio of 6.0. As a result, the ratio of specific heats (γ) was assumed to be a constant 1.2 for all CFD analysis. The secondary flow was modeled as a fixed massflux boundary with a total temperature of 1600 °R which is based on rocket pre-burner conditions.

Great care was taken to insure that the CFD results had adequate spatial resolution. A grid sensitivity study was performed which showed that the results were insensitive to grid spacing. A detailed discussion of the mesh generation methodology and NPARC configuration can be found in Ref. 15.

RESULTS AND DISCUSSION

CFD RESULTS

For a more detailed discussion of the details for the CFD analysis the reader is encouraged to examine Ref. 15. However, a brief summary is included in the following section to highlight some of the flow characteristics which affect system performance.

Figure 2 shows a representative Mach number distribution for case 28. Just downstream of the rocket nozzle exit is the free expansion of the plume to the mixer-ejector wall. The plume consists of both a shear layer and oblique shock structure. Next, the rocket plume impinges on the mixer-ejector wall. As the flow turns parallel to the wall, a reflected oblique shock is created which propagates toward the centerline. In some cases, the mixer-ejector is short enough that the oblique shocks do not meet at the center line before crossing the nozzle exit plane. However, if the duct is long enough, the oblique shocks reflect at the centerline, creating a diamond like structure in the flow. Also, as seen in the plot, when the oblique shocks impinge upon the wall, shock induced boundary layer separations are formed. Weak secondary expansion and shock waves can also be seen in the flow. Substantial boundary layer growth is also present in many of the solutions, especially for the longer mixer-ejectors. All cases exhibit some flow stratification and flowfield distortion at the mixer-ejector exit. Table IV presents both the full-flow and the gas generator CFD results and efficiencies based on isentropic performance.

REGRESSION RESULTS

FULL FLOW MODEL

Table V presents the results from the curvilinear regression analysis of the full thirty-six case model based on the full flow analysis. For this analysis the student's t constant was based on an estimate of a 95 percent confidence level for the error (E) term.

The resulting expression (12) is:

$$\eta I_{sp-FF} = 89.325 + 0.350\left[\frac{Pc-750}{450}\right] - 1.615\left[\frac{\frac{A_3}{A^*}-120}{80}\right] - 0.697\left[\frac{\frac{L}{D_3}-3.5}{1.5}\right] + 1.608\left[\frac{\frac{A_6}{A_3}-1.5}{0.5}\right]$$

$$+ 3.206\left[\frac{\varepsilon_r-12}{8}\right] + 0.334\left[\frac{Pc-750}{450}\right]\left[\frac{\frac{A_3}{A^*}-120}{80}\right] + 0.363\left[\frac{\frac{A_3}{A^*}-120}{80}\right]\left[\frac{m_s-4}{4}\right] - 0.421\left[\frac{m_s-4}{4}\right]$$

$$\times\left[\frac{\frac{A_6}{A_3}-1.5}{0.5}\right] - 0.723\left[\frac{m_s-4}{4}\right]\left[\frac{\varepsilon_r-12}{8}\right] + 0.283\left[\frac{\frac{A_3}{A^*}-120}{80}\right]\left[\frac{\frac{A_6}{A_3}-1.5}{0.5}\right] - 0.406\left[\frac{\frac{A_6}{A_3}-1.5}{0.5}\right]\left[\frac{\varepsilon_r-12}{8}\right]$$

$$- 1.586\left[\frac{\varepsilon_r-12}{8}\right]^2$$

Along with five linear relationships, several interactions and one second order relationship were found to affect Isp efficiency. For the linear terms the sign of the coefficient is an indication of whether the effect was positive or negative. The linear terms show increases in performance resulted from increases in chamber pressure, mixer-ejector area ratio, and rocket area ratio. These relationships can be seen by examining several pairs of data. The effect of chamber pressure can be seen by comparing cases 2 with 13 and 4 with 12 where with all parameters except chamber pressure are constant. The increase in performance due to an increase in mixer-ejector area ratio can be seen by comparing any of the following cases: 4 and 14, 7 and 21, and 15 and 6. The increase in performance with rocket area ratio can be seen by comparing cases 4 with 19 and 7 with 35. Performance was found to decrease with increasing mixer-ejector inlet area ratio and mixer-ejector length-to-diameter ratio. The effect of increasing mixer-ejector inlet area ratio can be seen by comparing any of the following cases: 1 with 16, 8 with 22, and 35 with 15. A detailed discussion of the linear relationships can be found in Ref. 8. For the interaction terms the sign only determines the bilinear variation. The performance is still highly dependent on the linear terms of the parameters involved in the interaction. Therefore, while the interaction may cause a decrease in performance, the gain from the linear term may be enough to cause a net increase in performance due to that parameter.

The first interaction is between chamber pressure and mixer-ejector inlet area ratio (Fig. 3). For Figs. 3 to 12, all parameters except the interaction discussed are at the mid level values. As mixer-ejector inlet area ratio is increased, the performance of the system decreases; likewise as chamber pressure increases performance increases. The effect of chamber pressure is minimal at lower mixer-ejector inlet area ratios, but becomes more pronounced as mixer-ejector inlet area ratio increases. The highest performing configuration is at the lowest mixer-ejector inlet area ratio possible and is unaffected by chamber pressure. An increased mixer-ejector inlet area ratio results in an larger free expansion between the rocket nozzle exit and mixer-ejector wall, hence a decrease in performance.

The second interaction is between mixer-ejector inlet area ratio and secondary flow (Fig. 4). As shown in the figure, between mixer-ejector inlet area ratios of 40 to 120, increasing secondary flow will decrease performance. For mixer-ejector inlet area ratios in the range of 120 to 200 an increase in secondary flow increases the efficiency. The general trends presented by Fig. 4 show that the larger mixer-ejector inlet areas produces the worst performance and adding secondary flow only slightly affects the results. As with the first interaction, increasing mixer-ejector inlet area ratio decreases performance.

The next interaction is between secondary flow and mixer-ejector area ratio. Figure 5 shows graphically how the interactions are related to Isp efficiency. For a straight mixer-ejector with a area ratio of 1.0 up to a mixer-ejector area ratio of 1.5 the performance increases with increasing secondary flow. However, at mixer-ejector area ratios higher than 1.5, the performance decreases as the secondary flow is increased. At constant secondary flows, as mixer-ejector area ratio is increased the performance increases.

The fourth interaction is between secondary flow and rocket area ratio (Fig. 6). This is an interaction with a curved shape due to the second order effect of rocket area ratio. As the figure shows, performance increases as secondary flow increases for constant rocket area ratios up to 12. However, at a rocket area ratios above 12, a reduction in performance is evident as secondary flow is increased. If secondary flow is held constant, increasing rocket area ratio will increase performance. For this interaction, the highest performance results from having the largest rocket area ratio with the least amount of secondary flow.

The fifth interactive relationship is between mixer-ejector inlet area ratio and mixer-ejector area ratio (Fig. 7). As with the linear relationships, increasing mixer-ejector inlet area ratio decreases performance while increasing mixer-ejector area ratio increases performance. This interaction is the balance between increasing the free expansion (A_3/A^*) and increasing the total nozzle surface (A_6/A_3) available for producing thrust. At constant mixer-ejector inlet area ratio the performance increases with increasing mixer-ejector area ratio. The most efficient configuration is with the smallest mixer-ejector inlet area ratio and the maximum mixer-ejector area ratio.

The final significant interaction is between mixer-ejector area ratio and rocket area ratio (Fig. 8). This is an interaction with a curved shape due to the second order effect of rocket area ratio. The performance increases as both rocket area ratio and mixer-ejector area ratio increase. For constant rocket area ratios, performance increases as mixer-ejector area ratio increases. The effect of increasing mixer-ejector area ratio is greater at lower rocket area ratios. Performance also increases at constant mixer-ejector area ratios for an increasing rocket area ratio. The highest performance can be obtained with the largest rocket area ratio and the largest mixer-ejector area ratio.

A second order effect is related to rocket area ratio (Fig. 9). In the linear model, as rocket area ratio increased performance increased according to the slope determined by the linear coefficient. However, due to the second-order effect the performance begins to level off as rocket area ratio approaches 20. This type of performance curve is similar to a standard performance versus area ratio curve for ideal nozzles showing diminishing returns as area ratio increases, a combination of a positive linear and negative curvilinear effects.

GAS-GENERATOR MODEL

Table VI presents the results from the curvilinear regression analysis of the full thirty-six case model based on the gas generator analysis. For this analysis the student's t constant was based on an estimate of a 95 percent confidence level for the error (E) term.

The resulting expression (13) is:

$$\eta I_{sp-GG} = 92.883 + 0.351\left[\frac{Pc-750}{450}\right] + 3.489\left[\frac{m_s-4}{4}\right] - 1.667\left[\frac{\frac{A_3}{A^*}-120}{80}\right] - 0.725\left[\frac{\frac{L}{D_3}-3.5}{1.5}\right]$$

$$+ 1.653\left[\frac{\frac{A_6}{A_3}-1.5}{0.5}\right] + 3.307\left[\frac{\varepsilon_r-12}{8}\right] + 0.347\left[\frac{Pc-750}{450}\right]\left[\frac{\frac{A_3}{A^*}-120}{80}\right] + 0.317\left[\frac{m_s-4}{4}\right]\left[\frac{\frac{A_3}{A^*}-120}{80}\right]$$

$$- 0.374\left[\frac{m_s-4}{4}\right]\left[\frac{\frac{A_6}{A_3}-1.5}{0.5}\right] - 0.619\left[\frac{m_s-4}{4}\right]\left[\frac{\varepsilon_r-12}{8}\right] + 0.283\left[\frac{\frac{A_3}{A^*}-120}{80}\right]\left[\frac{\frac{A_6}{A_3}-1.5}{0.5}\right]$$

$$- 0.426\left[\frac{\frac{A_6}{A_3}-1.5}{0.5}\right]\left[\frac{\varepsilon_r-12}{8}\right] - 1.639\left[\frac{\varepsilon_r-12}{8}\right]^2$$

Several interactions and one second order relationship were found to affect Isp efficiency. In fact, the same interactions were found to be significant in the gas-generator and full-flow models. However, the addition of secondary flow as a linear effect made a significant change in the plots for the interactions of the gas-generator model as compared to the full-flow analysis. For the interactions that do not involve secondary flow, the plots and relationships are similar to those discussed in the full flow analysis but the absolute values of the efficiency has changed. Due to the similarity in results only the interactions that involve secondary flow will be discussed in the following section. For comparison purposes the figures for the nonsecondary flow cases have been included. Figure 10 presents the interaction between mixer-ejector inlet area ratio and chamber pressure. Fig. 11 presents the interaction between mixer-ejector area ratio and mixer ejector inlet area ratio. Fig. 12 presents the interaction between rocket area ratio and mixer-ejector area ratio, and Fig. 13 presents the second order effect of rocket area ratio.

Figure 14 presents the interaction between secondary flow and mixer-ejector inlet area ratio. Due to the linear relationship of secondary flow for the gas generator analysis, this interaction is different than for the full-flow analysis. For a constant secondary flow value, increasing A_3/A^* decreases performance while at a constant A_3/A^*, increasing secondary flow increases performance. The general trends presented by Fig. 14 shows that the smallest mixer-ejector inlet area and largest secondary flow produces the highest performance.

The next interaction is between secondary flow and mixer-ejector area ratio (Fig.15). At constant secondary flows, as mixer-ejector area ratio is increased the performance increases. Performance also increases when secondary flow increases at constant mixer-ejector area ratios. For this system, the highest performance occurs with the largest mixer-ejector area ratios, hence the largest total area ratio for a given configuration, and routing the maximum amount of secondary flow into the engine. Due to the addition of secondary flow as a significant linear effect, this result is in direct contrast to Fig. 9 from the full-flow analysis.

The fourth interaction is between secondary flow and rocket area ratio (Fig. 16). This is an interaction with a curved shape due to the second order effect of rocket area ratio. The plot clearly shows that as either secondary flow or rocket area ratio increases, Isp efficiency increases. The highest performance occurs when both parameters are at the maximum values within the trade space. This is a result of the individual positive linear relationships driving the final results. From the results it is clear that for the gas generator analysis, the highest performance results from increasing rocket area ratio with an additional gain resulting from increasing secondary flow.

DISCUSSION OF RESULTS

Several facts are evident from examining the results from both the full-flow and gas generator methods of analyses. First, the assumption of a full-flow or gas generator cycle is important in determining which parameters have the most significant effect on performance. In the gas generator assumption, the addition of secondary flow is not only a strong main linear effect but also influences several of the interactions. As a result, if a gas generator system is used or extra propellants are required to cool the vehicle, all of the fluids should be routed back into the RBCC engine system. This is not unexpected since any gain in performance is better than venting the propellants overboard.

In both data sets, the initial rocket area ratio is one of the most influential parameters because it not only has the largest and most significant linear effect, it is the only second order effect and appears in several interactions. A larger rocket area ratio also reduces the size of the free expansion inside of the engine and hence reduces the potential for additional losses. A comparison of the Mach number CFD plots from cases 4 and 19 (Fig. 17) shows how the change in rocket area ratio affects the flow field. In case 19 with the larger rocket exit area ratio both the mixer-ejector and rocket exit Mach numbers are greater than those found in case 4. The rocket exhaust plume and initial reflected shock structure also extend farther downstream for the cases with a larger rocket. There are also fewer reflected shock boundary layer interactions and smaller regions of slower moving flow at the exit with the larger rocket area ratio. However, the most important factor is the efficiency gained by the initial expansion along the rocket nozzle as opposed to a free expansion.

A corresponding increase in performance results from an increase in mixer ejector area ratio. This increase is simply due to the increase in total area ratio available for expansion. The Mach number CFD plots from cases 4 and 14 (Fig. 18) shows how the change in mixer-ejector area ratio affects the flow field holding all other parameters constant. Because some this expansion occurs on the diverging mixer-ejector wall, there are fewer losses than if the expansion went to the same exit area ratio for a straight duct. The losses associated with the A_6/A_3 expansion are due to divergence losses and boundary layer development which are generally small by comparison to the losses due to the free expansion. From the Mach contour plot of Fig. 18 several differences are evident. The diverging case has a longer initial plume expansion and the reflected waves are longer, result in fewer waves in the mixer-ejector nozzle. Overall the diverging mixer-ejector has higher exit Mach numbers which translate to increased momentum. The net effect is increased efficiency for cases where the mixer-ejector section diverges.

The amount of free expansion between the rocket and mixer-ejector wall is also directly related to the mixer-ejector inlet area ratio. In both sets of analyses, all linear relationships and interactions that involve this parameter provide increased performance when A_3/A^* is minimized. A comparison of the CFD Mach number contour plots from cases 8 and 22 (Fig. 19) shows how the change in mixer-ejector inlet area ratio affects the flow field. Initially, based upon previous comparisons, the large region of high speed flow and the fact that the reflected oblique shock does not impinge at the centerline, it would be expected that case 22 would be the higher performing of the configurations. However, it turns out that case 8 is the more efficient configuration. This is a direct result of the reduced free expansion for case 8 as compared to case 22. The free expansion appears to be the dominant feature in determining performance, more so than exit Mach number or the number of reflected shocks in the mixer-ejector nozzle.

One way to examine the effect of free expansion on performance is to look at the base pressure upstream of the rocket. When no secondary flow is present the system acts as a supersonic driven cavity where the primary rocket exhaust evacuates the cavity forward of the rocket. The result is a low base pressure which provides a small amount of thrust for the area between the rocket nozzle exit and mixer ejector wall. An increase in thrust could be provided by increasing the base pressure. One method to increase base pressure is by introducing secondary flow into the cavity. But as we have shown with the parameteric models, the gain in thrust must be balanced by the increase in net mass flow to the system. If the system calls for a full-flow cycle then the addition of a separate secondary flow system is not necessary to increase performance. However, if the gas generator cycle is selected or additional cooling flow is required, it is beneficial to route the tap-off gases into the cavity and overall performance increases.

Adding secondary flow to the system also effects the primary rocket exhaust expansion. The primary rocket expansion is a function of the cavity pressure along with the nozzle exit divergence angle and nozzle exit static pressure. Secondary flow is used to increase the ambient pressure into which the primary flow expands. By increasing the pressure, the plume expansion angle is reduced and the flow is turned more in the axial direction, resulting in lower divergence losses due to the reflected oblique shock angle. This is evident by examining the particle trace and nondimensional pressure profile plots for cases 4 and 20 (Fig. 20).[15] In case 4 with no

secondary flow the primary flow from the rocket nozzle has a steep exit angle and the flow impacts the mixer-ejector wall at a steep angle. The plots also show that with no secondary flow, several recirculation zones are present inside of the cavity. However, in case 20 with 8 percent injected secondary flow the rocket plume is turned more axially along the flow path and impinges the mixer-ejector wall at a much shallower angle. Case 20 also shows that when secondary flow is added only one small eddy is present near the impingement point of the primary stream. The non-dimensional pressure profiles show that the impingement point is moved farther downstream with the addition of secondary flow. The result is an increased efficiency due to fewer reflected shocks. It can also be seen by examining the oblique shock tables that reducing the oblique shock angle increases the downstream Mach number. The hypothesis is that reducing the total exit angle and the wall impingement angle is one mechanism that contributes to increasing performance.

Finally, for comparison, the predicted results from the curvilinear models were compared to the actual values from the CFD results. As shown by the results in Table VII, the actual values for both models agree well with the model predicted values. The fact is also evident by the low calculated error term for the curvilinear model, at a 95 percent confidence level.

CONFIRMATION CASES

For a check of model accuracy for both the full-flow analysis and gas-generator analysis, eight confirmation CFD cases were run. The input variables for the cases can be found in Table VIII. Cases 37-40 were selected to examine the interaction between secondary flow and mixer-ejector area ratio, as a result those values were varied between the high and low inputs while all other variables were maintained at the mid-point. Cases 41-44 were selected to examine the interaction between secondary flow and rocket exit area ratio, as a result those values were also varied between the high and low inputs while all other variables were maintained at the mid-point. The results from the CFD and models can be found in table IX. The results are similar for both the full-flow and gas generator analysis where, except for one case, the percent difference between CFD and model predictions fall well within the error term from the original model. Theses results are further evidence of the robust nature of the curvilinear model.

OPTIMUM CONFIGURATION

An optimum configuration was determined for this type of axisymmetric configuration using the curvilinear models based upon both the full-flow and gas-generator assumptions. For the full-flow assumption the following configuration will optimize performance:

Chamber pressure (psi)	1152.9
Rocket area ratio (ε_R)	20
Percent of secondary flow (m_s)	0.25
Mixer-ejector inlet area ratio[A_3/A^*]	40
Mixer-ejector area ratio [A_6/A_3](ε_{ME})	1.98
Mixer-ejector length-to-diameter ratio [L/D_3].	3.54

The results from the optimization serve to reinforce the relationships shown in the curvilinear model. In general, the positive linear relationships are at or near the maximum set point while the negative linear relationships are at or near the minimum set point. However, some of the relationships are affected by the interactions. The highest performance is obtained with a near maximum chamber pressure, a maximum rocket area ratio, and a near maximum mixer-ejector area ratio Even though there was no linear effect, the amount of secondary flow required to increase performance is very small, most likely due to the multiple interactions involving that parameter. The optimum performance is obtained when the mixer-ejector area ratio is at a minimum. The mixer-ejector length-to-diameter ratio does not follow the same pattern as the other parameters, instead optimum performance is achieved near the mid-point value.

For the gas-generator assumption the following configuration will optimize performance:

Chamber pressure (psi)	998.4
Rocket area ratio (ε_R)	18.6
Percent of secondary flow (m_s)	8.0

Mixer-ejector inlet area ratio[A_3/A^*]	40
Mixer-ejector area ratio [A_6/A_3](ε_{ME})	2.0
Mixer-ejector length-to-diameter ratio [L/D_3].	2.04

As with the full-flow model, the results from the optimization serve to reinforce the relationships shown in the curvilinear model. In general, the positive linear relationships are at or near the maximum set point while the negative linear relationships are at or near the minimum set point. However, some of the relationships are affected by the interactions and the addition of secondary flow as a significant linear effect obviously changes the results. The highest performance is obtained with a near maximum rocket area ratio, a maximum amount of secondary flow, and a maximum mixer-ejector area ratio. Chamber pressure is still a high value, however it is nearly 200 psi below the maximum value. The optimum performance is obtained when the mixer-ejector area ratio and mixer-ejector length-to-diameter ratio are at the minimum.

CONCLUDING REMARKS

Results from the regression revealed several significant interactions between the parameters and second order effects. Results were analyzed based on both full flow and gas generator systems. The significant linear relationships are:

- Increasing chamber pressure increases specific impulse efficiency.
- Increasing mixer-ejector inlet area ratio decreases specific impulse efficiency.
- Increasing mixer-ejector length-to-diameter area ratio decreases specific impulse efficiency.
- Increasing mixer-ejector area ratio increases specific impulse efficiency.
- Increasing rocket area ratio increases specific impulse efficiency.

For the full flow analysis, secondary flow was not a significant linear effect, however it was a significant linear effect in the gas generator analysis. The interactions were consistent between models, although with different coefficients. The addition of secondary flow in the gas generator analysis as a significant linear effect did change the relationship of the interactions involving secondary flow as compared to the full flow analysis. The six significant interactions were:

- Chamber pressure with mixer-ejector inlet area ratio
- Injected secondary flow percentage with mixer-ejector inlet area ratio
- Injected secondary flow percentage with mixer-ejector exit area ratio
- Injected secondary flow percentage with rocket exit area ratio
- Mixer-ejector inlet area ratio with mixer ejector exit area ratio
- Mixer-ejector exit area ratio with rocket exit area ratio

Rocket exit area ratio was found to provide a negative second order effect which resulted in diminishing returns for specific impulse efficiency with increasing rocket area ratio. All of the interactions and second order effects served to enhance the results from the linear analysis while providing a more accurate parametric model. Results from the curvilinear model were shown to correspond very well with the CFD results. The parametric equations developed provide a first-order analysis tool to evaluate the mode 4 performance of an RBCC engine.

The CFD results showed several areas of concern in the flow path which ultimately had an affect on the parametric model. These flow characteristics include the free expansion from the rocket nozzle to mixer-ejector wall, reflected oblique shock structures through out the flow path, shock induced boundary layer separations, thick boundary layer development at the exit, and flowfield divergence at the exit. Injected secondary flow was used in an attempt to increase performance, however it was found to be dependent on the system assumptions. CFD particle trace results showed that injected secondary flow influenced the flow stream by altering the free expansion angle of the rocket plume as well as reducing the cavity recirculation zones.

Finally, this study has shown that utilizing design of experiments is an effective tool to maximize results while reducing the number of experiments require

REFERENCES

1. Escher, W.J.D.; Teeter, R.R.; and Rice, E.E.: Air-breathing and Rocket Propulsion Synergism: Enabling Measures for Tomorrow's Orbital Transports. AIAA 86–1680, June 1986.
2. Kors, D.L.: Combined Cycle Propulsion for Hyper-sonic Flight. IAF–87–263, October 1987.
3. Foster, R.W.; Escher, W.J.D.; and Robinson, J.W.: Studies of an Extensively Axisymmetric Rocket Based Combined Cycle (RBCC) Engine Powered SSTO Vehicle. AIAA 89–2294, July 1989.
4. Lepsch Jr., R.A.; and Naftel, J.C.: The Performance of a Winged Booster Powered by Combined Rocket and Airbreathing Propulsion. AIAA 92–3500, July 1992.
5. Escher, W.J.D.; and Czysz, P.A.: Rocket-Based Combined Cycle Powered Spaceliner Concept. IAF–93–S.4.478, October 1993.
6. Escher, W.J.D.; Hyde, E.H.; and Anderson, D.M.: A User's Primer for Comparative Assessments of All-Rocket and Rocket-Based Combined-Cycle Pro-pulsion Systems for Advanced Earth-to-Orbit Space Transport Applications. AIAA 95–2472, July 1995.
7. Bulman, M.; and Siebenhaar, A.: The Strutjet Engine: Exploding the Myths Surrounding High Speed Air-breathing Propulsion. AIAA 95–2475, July 1995.
8. Smith, T.D., Steffen Jr., C.J., Yungster, S., and Keller, D.J.: Performance of an Axisymmetric Rocket Based Combined Cycle Engine During Rocket Only Operation Using Linear Regression Analysis. NASA TM–206632, March 1998.
9. Rao, G.V.R.: Optimum Thrust Performance of Contoured Nozzles. Chemical Propulsion Information Agency, JANAF Liquid Propellant Group 1st Meeting, November 1959, pp. 243–259.
10. Tuttle, J.L.; and D.H. Blount: Perfect Bell Nozzle Parametric and Optimization Curves. NASARP–1104, 1983.
11. Anon., NPARC User's Guide Version 3.0, the NPARC Alliance, September 1996.
12. Nickerson, G.R.; Dang, A.L.; and Dunn, S.S.: The Rao Method Optimum Nozzle Contour Program. NAS8–36863, 1988.
13. Beyer, W.H., editor: *CRC Standard Mathematical Tables, 28th Edition*. CRC Press, Inc., 1987.
14. Spalart, P.R.; and Allmaras, S.R.: A One-Equation Turbulence Model for Aerodynamic Flows. AIAA 92–0439, 1992.
15. Steffen Jr., C.J.; Smith, T.D.; Yungster, S.; and Keller, D.J.: Rocket Based Combined Cycle Analysis using NPARC. AIAA 98–0954, January 1998.
16. Gordon, S.; and McBride, B.J.: *Computer Program for Calculation of Complex Chemical Equilibrium Compositions, Rocket Performance, Incident and Reflected Shocks, and Chapman-Jouguet Detonations*. NASA SP–273, 1971.

TABLE I.—RBCC ENGINE PARAMETERS AT THREE LEVELS

Chamber pressure (Pc) (psi)	300	750	1200
Rocket exit area ratio (ε_R)	4	12	20
Percent of injected secondary flow (m_s)	0.0	4.0	8.0
Mixer-ejector inlet area ratio[A_3/A^*]	40	120	200
Mixer-ejector area ratio [A_6/A_3](ε_{ME})	1.0	1.5	2.0
Mixer-ejector length-to-diameter ratio [L/D]	2.0	3.5	5.0

TABLE II.—DESIGN INPUT VARIABLES

Case	Chamber pressure, psi	Secondary flow percent	Mixer-ejector inlet area ratio	Length to diameter ratio	Mixer-ejector area ratio	Rocket area ratio	Total area ratio
	x_1	x_2	x_3	x_4	x_5	x_6	
1	300	8.0	40.0	2.0	2.0	4.0	80
2	300	0.0	40.0	5.0	2.0	20.0	80
3	1200	0.0	200.0	2.0	2.0	4.0	400
4	300	0.0	200.0	5.0	1.0	4.0	200
5	300	8.0	200.0	2.0	1.0	20.0	200
6	1200	8.0	200.0	5.0	2.0	20.0	400
7	1200	8.0	40.0	5.0	1.0	4.0	40
8	1200	0.0	40.0	2.0	1.0	20.0	40
9	750	4.0	120.0	3.5	1.5	12.0	180
10	300	0.0	200.0	2.0	2.0	20.0	400
11	1200	8.0	40.0	2.0	2.0	20.0	80
12	1200	0.0	200.0	5.0	1.0	4.0	200
13	1200	0.0	40.0	5.0	2.0	20.0	80
14	300	0.0	200.0	5.0	2.0	4.0	400
15	1200	8.0	200.0	5.0	1.0	20.0	200
16	300	8.0	200.0	2.0	2.0	4.0	400
17	300	8.0	40.0	5.0	2.0	20.0	80
18	1200	0.0	40.0	2.0	1.0	4.0	40
19	300	0.0	200.0	5.0	1.0	20.0	200
20	300	8.0	200.0	5.0	1.0	4.0	200
21	1200	8.0	40.0	5.0	2.0	4.0	80
22	1200	0.0	200.0	2.0	1.0	20.0	200
23	750	0.0	40.0	5.0	1.0	4.0	40
24	750	4.0	200.0	2.0	1.0	4.0	200
25	300	4.0	40.0	5.0	1.5	4.0	60
26	750	8.0	120.0	2.0	1.5	4.0	180
27	1200	0.0	200.0	5.0	1.5	12.0	300
28	300	4.0	120.0	5.0	1.0	12.0	120
29	300	8.0	40.0	3.5	1.0	4.0	40
30	300	0.0	120.0	2.0	1.0	4.0	120
31	300	4.0	40.0	2.0	1.0	20.0	40
32	1200	8.0	200.0	2.0	1.0	12.0	200
33	300	0.0	40.0	3.5	1.5	20.0	60
34	750	0.0	40.0	2.0	2.0	12.0	80
35	1200	8.0	40.0	5.0	1.0	20.0	40
36	1200	4.0	120.0	3.5	2.0	4.0	240

TABLE III.—CFD CONSTANT TOTAL CONDITIONS FROM A CHEMICAL EQUILIBRIUM CODE

Chamber pressure, psia	Molecular weight	Chamber temperature, °R
300	13.02	6200
750	13.19	6400
1200	13.27	6500

TABLE IV.—CFD SPECIFIC IMPULSE RESULTS AND CALCULATED ISENTROPIC SPECIFIC IMPULSE EFFICIENCIES

Case	Isp_{CFD}, sec	Isp isentropic full-flow, sec	Isp isentropic full-flow efficiency, percent	Isp isentropic gas-generator, sec	Isp isentropic gas-generator efficiency, percent
1	399.54	451.57	88.48	418.12	95.56
2	424.33	451.57	93.97	451.57	93.97
3	415.94	480.04	86.65	480.04	86.65
4	361.73	465.06	77.78	465.06	77.78
5	411.29	465.06	88.44	430.61	95.51
6	430.64	480.04	89.71	444.48	96.89
7	374.07	445.44	83.98	412.44	90.70
8	416.89	445.44	93.59	445.44	93.59
9	418.26	468.03	89.37	450.03	92.94
10	433.80	473.31	91.65	473.31	91.65
11	425.32	457.99	92.87	424.06	100.30
12	375.90	471.67	79.69	471.67	79.69
13	432.92	457.99	94.53	457.99	94.53
14	393.85	473.31	83.21	473.31	83.21
15	415.28	471.67	88.04	436.73	95.09
16	407.86	473.31	86.17	438.25	93.06
17	412.17	451.57	91.28	418.12	98.58
18	376.14	445.44	84.44	445.44	84.44
19	403.11	465.06	86.68	465.06	86.68
20	372.02	465.06	79.99	430.16	86.39
21	399.24	457.99	87.17	424.06	94.15
22	419.26	471.67	88.89	471.67	88.89
23	369.83	443.34	83.42	443.34	83.42
24	381.15	469.45	81.19	451.39	84.44
25	384.22	446.71	86.01	429.53	89.45
26	404.67	468.03	86.46	433.36	93.38
27	415.05	476.73	87.06	476.73	87.06
28	397.36	458.00	86.76	440.38	90.23
29	377.51	439.19	85.96	406.66	92.83
30	369.02	458.00	80.57	458.00	80.57
31	399.86	439.19	91.04	422.30	94.69
32	415.49	471.67	88.09	436.73	95.14
33	419.92	446.71	94.00	446.71	94.00
34	427.36	455.83	93.76	455.83	93.76
35	401.40	445.44	90.11	412.44	97.32
36	404.55	473.98	85.35	455.75	88.76

TABLE V.—MULTIPLE REGRESSION FOR AN ISENTROPIC FULL-FLOW SOLUTION
(R^2 = 0.985, $S_{Y\,X}$ = 0.6573, t = 1.71, E = ±1.13 PERCENT)

Term		Coefficient	Confidence level, percent
Constant	β_0	89.325	>99.99
Chamber pressure	β_1	0.350	99.16
Mixer-ejector inlet area ratio	β_2	–1.615	99.99
Mixer-ejector length-to-diameter ratio	β_3	–0.697	99.99
Mixer-ejector area ratio	β_4	1.608	99.99
Rocket area ratio	β_5	3.206	99.99
Chamber pressure *x* mixer-ejector inlet area ratio	β_7	0.334	98.46
Secondary flow *x* mixer-ejector inlet area ratio	β_{12}	0.363	98.89
Secondary flow *x* mixer-ejector area ratio	β_{14}	–0.421	99.53
Secondary flow *x* rocket exit area ratio	β_{16}	–0.723	99.99
Mixer-ejector inlet area ratio *x* mixer-ejector area ratio	β_{17}	0.283	95.53
Mixer-ejector area ratio *x* rocket exit area ratio	β_{21}	–0.406	98.45
(Rocket exit area ratio)^2	β_{27}	–1.586	99.98

TABLE VI.—MULTIPLE REGRESSION FOR AN ISENTROPIC GAS GENERATOR ANALYSIS
(R^2 = 0.999, $S_{Y\,X}$ = 0.703, t = 1.72, E = ±1.21 PERCENT)

Term		Coefficient	Confidence level, percent
Constant	β_0	92.8833	>99.99
Chamber pressure	β_1	0.351	98.69
Secondary flow	β_2	3.489	99.99
Mixer-ejector inlet area ratio	β_3	–1.667	99.99
Mixer-ejector length-to-diameter ratio	β_4	–0.725	99.99
Mixer-ejector area ratio	β_5	1.653	99.99
Rocket area ratio	β_6	3.307	99.99
Chamber pressure *x* mixer-ejector inlet area ratio	β_7	0.347	98.15
Secondary flow *x* mixer-ejector inlet area ratio	β_{12}	0.317	96.56
Secondary flow *x* mixer-ejector area ratio	β_{14}	–0.374	98.27
Secondary flow *x* rocket exit area ratio	β_{15}	–0.619	99.97
Mixer-ejector inlet area ratio *x* mixer-ejector area ratio	β_{17}	0.283	93.84
Mixer-ejector area ratio *x* rocket exit area ratio	β_{21}	–0.426	99.30
(Rocket exit area ratio)^2	β_{27}	–1.639	99.98

TABLE VII.—COMPARISON OF CFD RESULTS WITH THE CURVILINEAR MODEL RESULTS

Case	Full-flow, percent			Gas-generator, percent		
	CFD	Curvilinear model E = ±1.13 percent	Percent difference, percent	CFD	Curvilinear model E = ±1.21 percent	Percent difference percent
	Actual	Predicted		Actual	Predicted	
1	88.48	88.50	–0.02	95.56	95.54	0.02
2	93.97	94.27	-0.32	93.97	94.25	-0.30
3	86.65	85.93	0.82	86.65	86.01	0.74
4	77.78	77.73	0.06	77.78	77.69	0.12
5	88.44	87.92	0.59	95.51	94.96	0.58
6	89.71	90.02	–0.35	96.89	97.18	-0.30
7	83.98	84.52	–0.64	90.70	91.25	-0.61
8	93.59	93.02	0.61	93.59	93.08	0.55
9	89.37	89.33	0.07	92.94	92.88	0.09
10	91.65	91.61	0.05	91.65	91.61	0.05
11	92.87	92.69	0.19	100.30	100.07	0.23
12	79.69	79.10	0.74	79.69	79.08	0.77
13	94.53	94.30	0.24	94.53	94.26	0.28
14	83.21	83.17	0.05	83.21	83.16	0.06
15	88.04	87.89	0.17	95.09	94.91	0.19
16	86.17	85.89	0.32	93.06	92.71	0.38
17	91.28	91.26	0.02	98.58	98.61	-0.03
18	84.44	84.35	0.11	84.44	84.37	0.08
19	86.68	86.40	0.32	86.68	86.39	0.33
20	79.99	80.74	–0.94	86.39	87.28	-1.03
21	87.17	87.14	0.04	94.15	94.10	0.05
22	88.89	89.17	–0.31	88.89	89.24	-0.39
23	73.42	82.94	0.58	83.42	82.92	0.60
24	81.19	81.32	–0.16	84.4	84.63	-0.23
25	86.01	85.43	0.67	89.4	88.88	0.64
26	86.46	85.95	0.59	93.3	92.77	0.65
27	87.06	87.33	–0.31	87.0	87.38	-0.37
28	86.76	86.67	0.10	90.2	90.15	0.09
29	85.96	85.18	0.90	92.8	91.97	0.93
30	80.57	81.72	–1.43	80.5	81.75	-1.46
31	91.04	92.32	–1.41	94.69	96.00	-1.38
32	88.09	87.99	0.12	95.14	94.88	0.27
33	94.00	93.63	0.40	94.00	93.66	0.36
34	93.76	93.75	0.01	93.7	93.85	-0.10
35	90.11	90.30	–0.20	97.3	97.48	-0.16
36	85.35	86.90	–1.81	88.7	90.37	-1.81

TABLE VIII.—DESIGN INPUT VARIABLES FOR MODEL CONFIRMATION CASES

Case	Chamber pressure psi	Secondary flow percent	Mixer-ejector inlet area ratio	Length to diameter ratio	Mixer-ejector area ratio	Rocket area ratio	Total area ratio
	x_1	x_2	x_3	x_4	x_5	x_6	
37	750	0.0	120	3.5	2.0	12	240
38	750	0.0	120	3.5	1.0	12	120
39	750	8.0	120	3.5	2.0	12	240
40	750	8.0	120	3.5	1.0	12	120
41	750	0.0	120	3.5	1.5	20	180
42	750	0.0	120	3.5	1.5	4	180
43	750	8.0	120	3.5	1.5	20	180
44	750	8.0	120	3.5	1.5	4	180

TABLE IX.—COMPARISON OF CFD RESULTS WITH THE CURVILINEAR MODEL RESULTS FOR MODEL CONFIRMATION CASES

Case	Full-flow, percent			Gase generator, percent		
	CFD	Curvilinear model, E = ±1.13 percent	Percent difference	CFD	Curvilinear model, E = ±1.21 percent	Percent difference
	Actual	Predicted		Actual	Predicted	
37	89.94	91.35	-1.57	89.94	91.42	-1.64
38	86.98	87.30	-0.37	86.98	87.37	-0.45
39	89.65	90.51	-0.97	96.82	97.65	-0.86
40	87.58	88.14	-0.64	94.59	95.09	-0.53
41	91.29	91.67	-0.42	91.29	91.68	-0.43
42	83.46	83.81	-0.42	83.46	83.83	-0.45
43	89.69	90.22	-0.60	96.86	97.42	-0.58
44	85.39	85.26	0.15	92.22	92.05	0.19

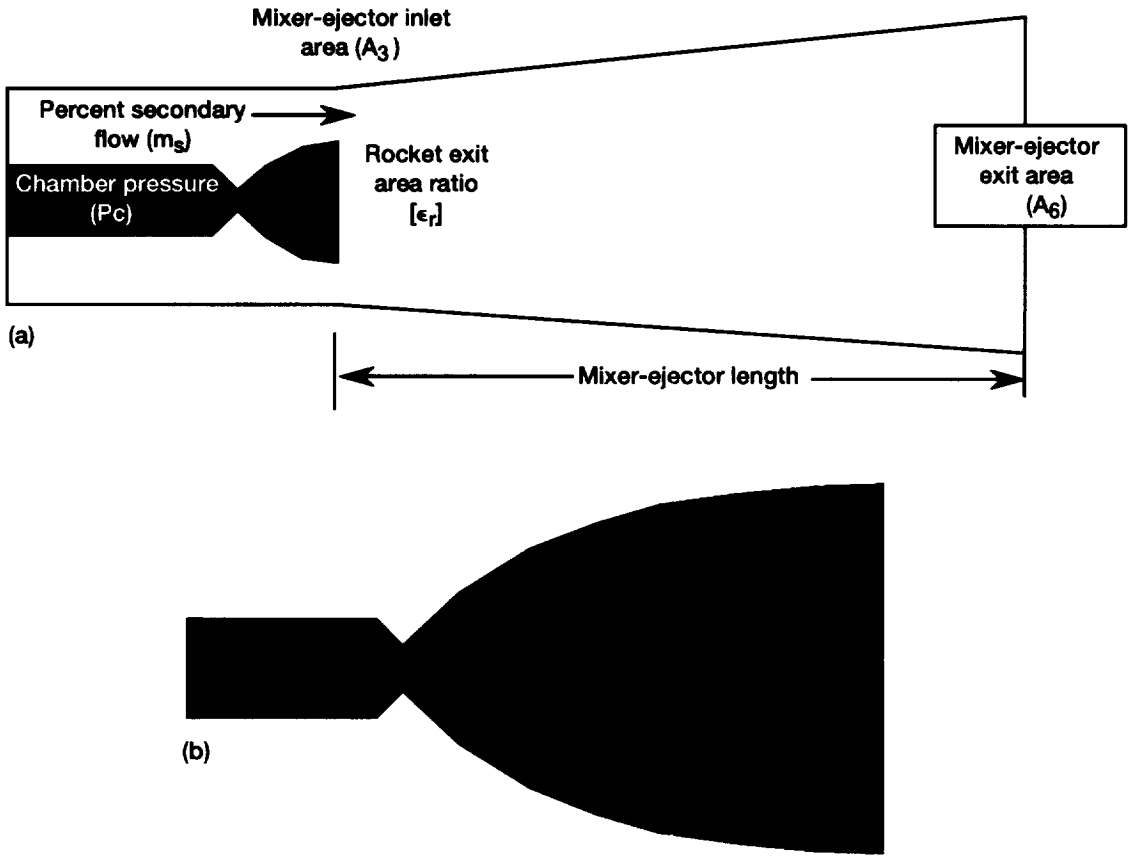

Figure 1.—(a) Axisymmetric configuration. (b) Optimized rocket nozzle configuration.

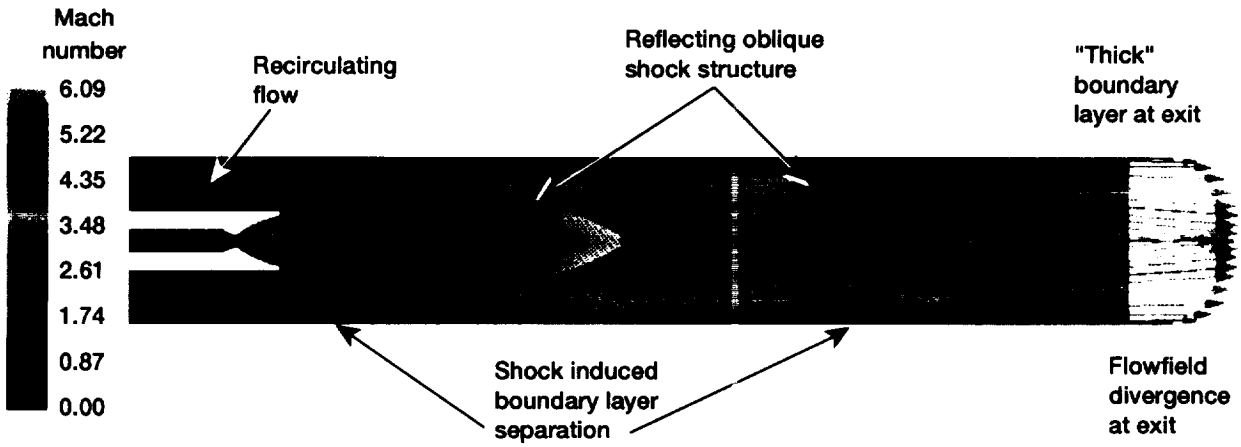

Figure 2.—Mach number contour plot for case 28 highlighting a representative flow structure.

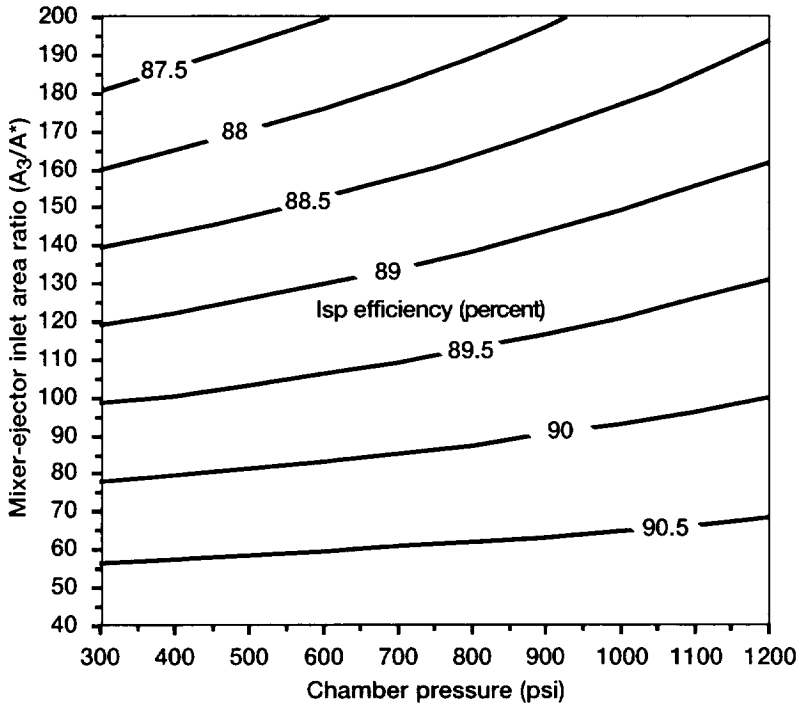

Figure 3.—Full flow analysis-mixer-ejector inlet area ratio as a function of chamber pressure. (Baseline: Pc = 750 psia, $\dot{m}_s$ = 4%, A_3/A^* = 120, L/D_3 = 3.5, A_6/A_3 = 1.5, ϵ_r = 12).

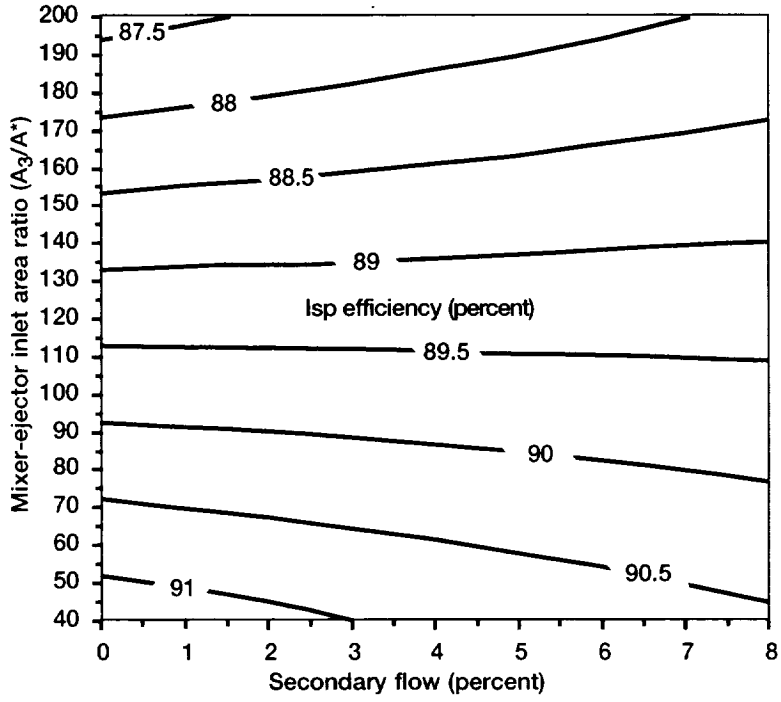

Figure 4.—Full flow analysis-mixer-ejector inlet area ratio as a function of secondary flow. (Baseline: Pc = 750 psia, m_s = 4%, A_3/A^* = 120, L/D_3 = 3.5, A_6/A_3 = 1.5, ϵ_r = 12).

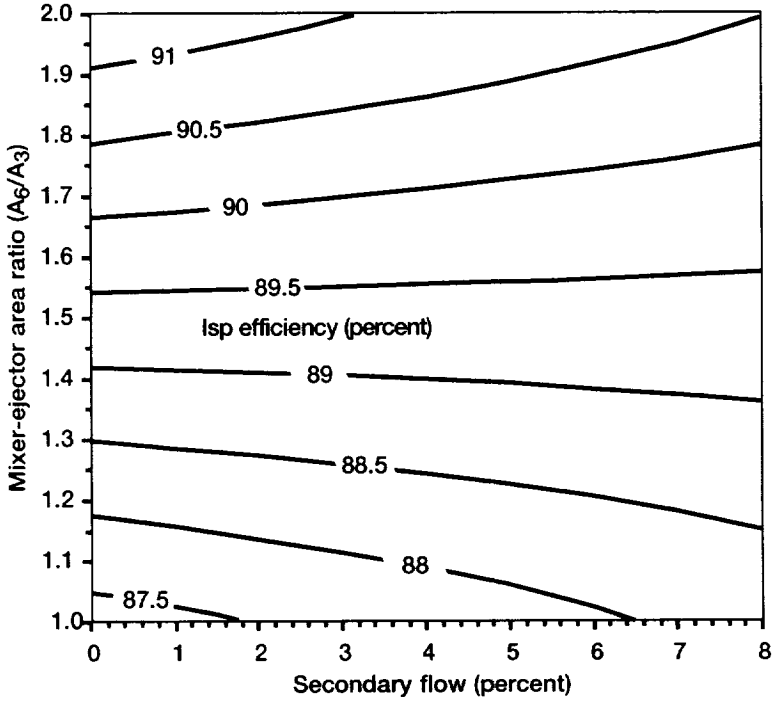

Figure 5.—Full flow analysis-mixer-ejector area ratio as a function of secondary flow. (Baseline: Pc = 750 psia, m_s = 4%, A_3/A^* = 120, L/D_3 = 3.5, A_6/A_3 = 1.5, ϵ_r = 12).

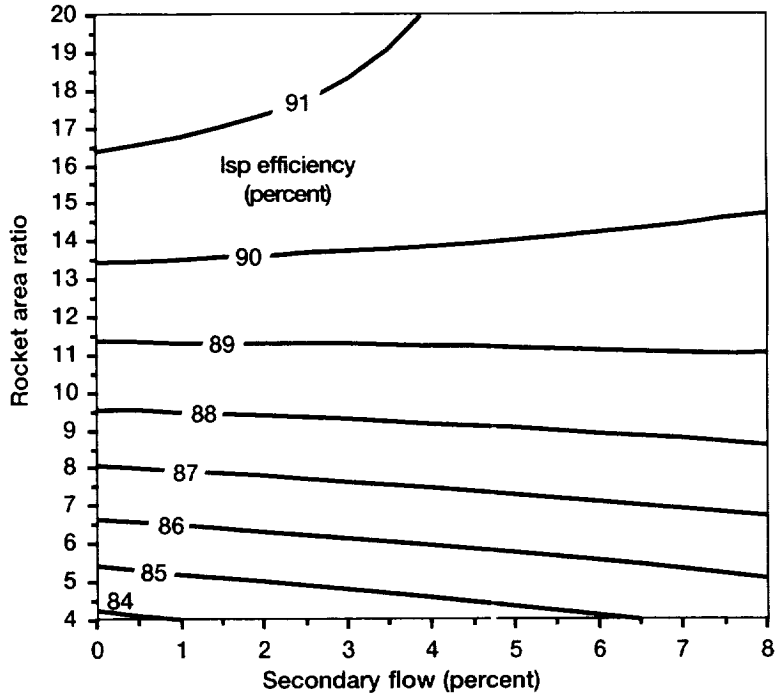

Figure 6.—Full flow analysis-rocket area ratio as a function of secondary flow. (Baseline: Pc = 750 psia, m_s = 4%, A_3/A^* = 120, L/D_3 = 3.5, A_6/A_3 = 1.5, ϵ_r = 12).

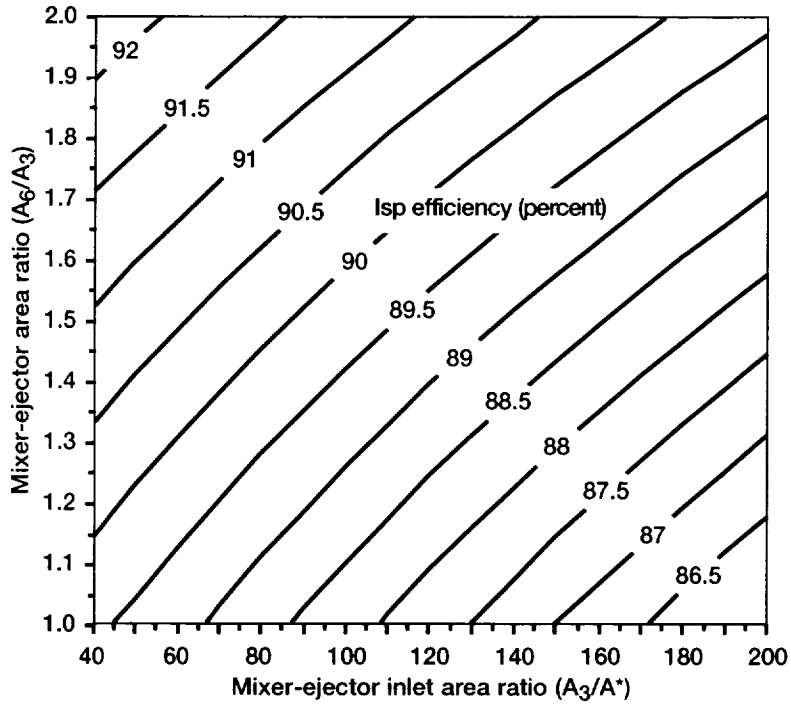

Figure 7.—Full flow analysis-mixer-ejector area ratio as a function of mixer-ejector inlet area ratio. (Baseline: Pc = 750 psia, m_s = 4%, A_3/A^* = 120, L/D_3 = 3.5, A_6/A_3 = 1.5, ϵ_r = 12).

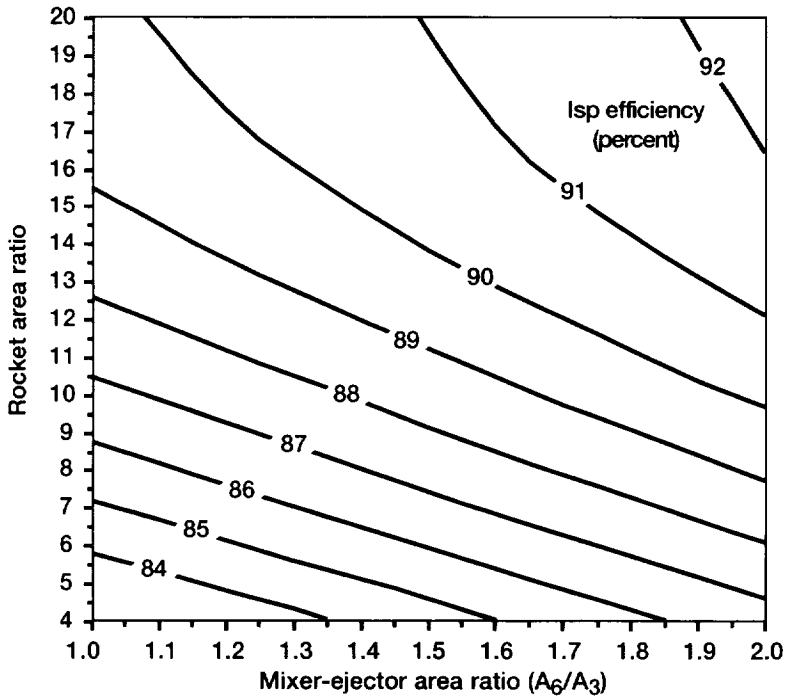

Figure 8.—Full flow analysis-rocket area ratio as a function of mixer-ejector area ratio. (Baseline: Pc = 750 psia, m_s = 4%, A_3/A^* = 120, L/D_3 = 3.5, A_6/A_3 = 1.5, ϵ_r = 12).

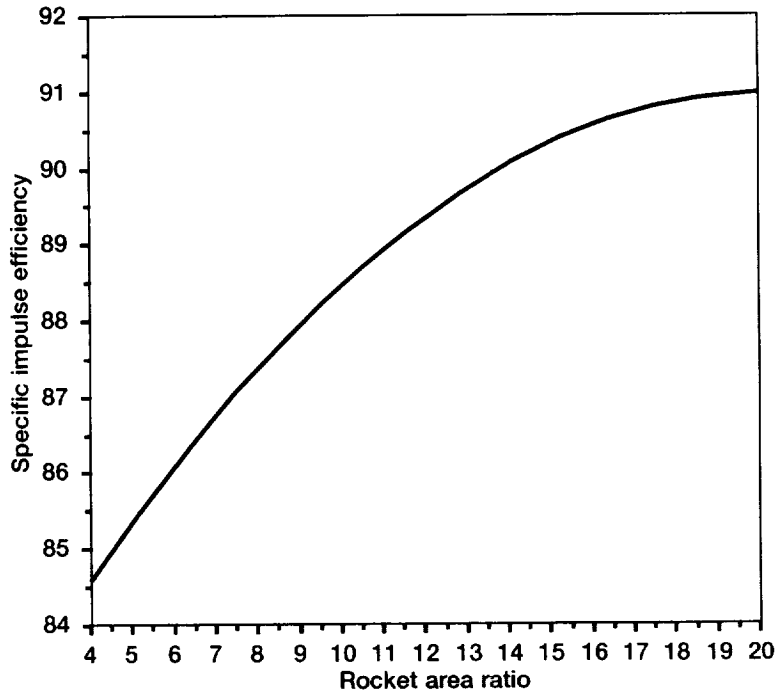

Figure 9.—Full flow analysis-specific impulse efficiency as a function of rocket area ratio. (Baseline: Pc = 750 psia, m_s = 4%, A_3/A^* = 120, L/D_3 = 3.5, A_6/A_3 = 1.5, ϵ_r = 12).

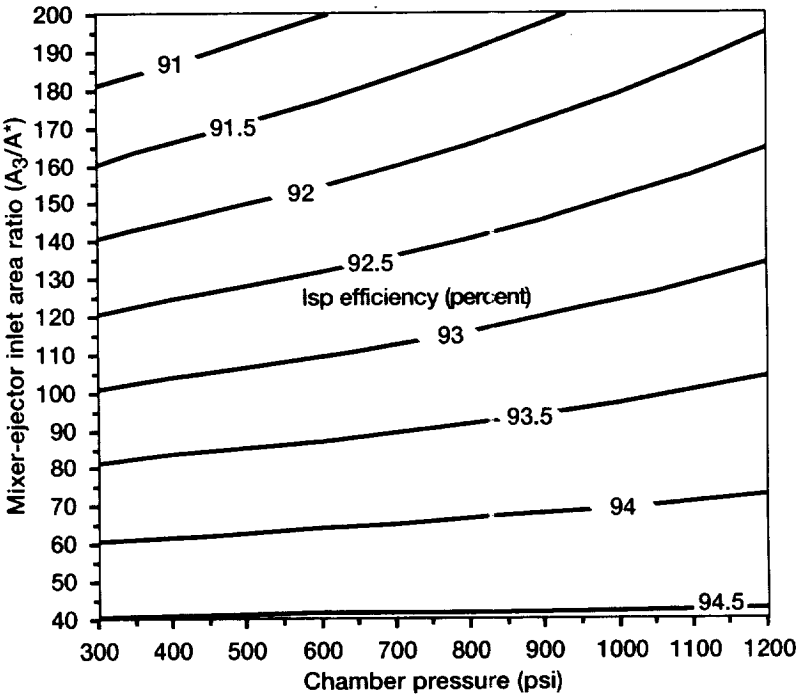

Figure 10.—Gas generator analysis-mixer-ejector inlet area ratio as a function of chamber pressure. (Baseline: Pc = 750 psia, m_s = 4%, A_3/A^* = 120, L/D_3 = 3.5, A_6/A_3 = 1.5, ϵ_r = 12).

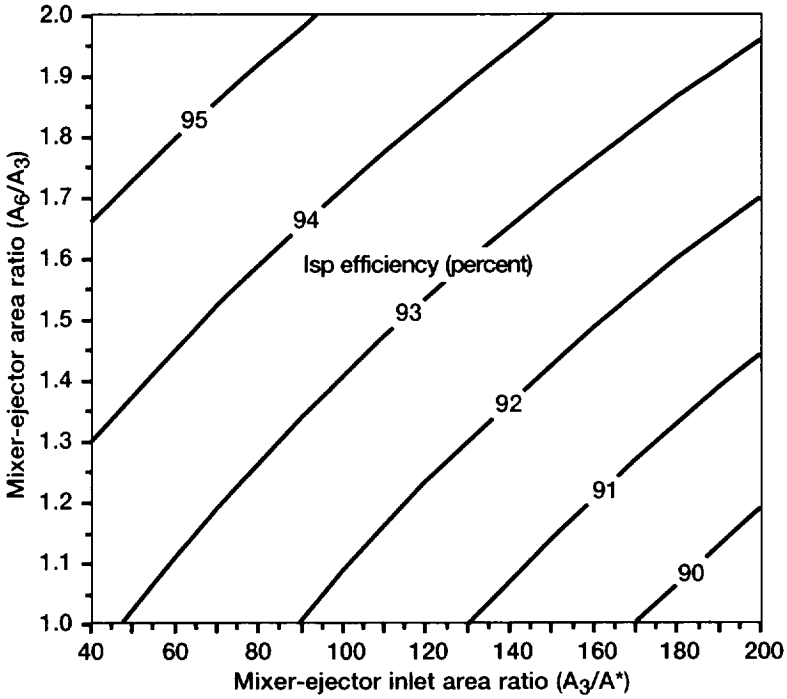

Figure 11.—Gas generator analysis-mixer-ejector area ratio as a function of mixer-ejector inlet area ratio. (Baseline: Pc = 750 psia, m_s = 4%, A_3/A^* = 120, L/D_3 = 3.5, A_6/A_3 = 1.5, ϵ_r = 12).

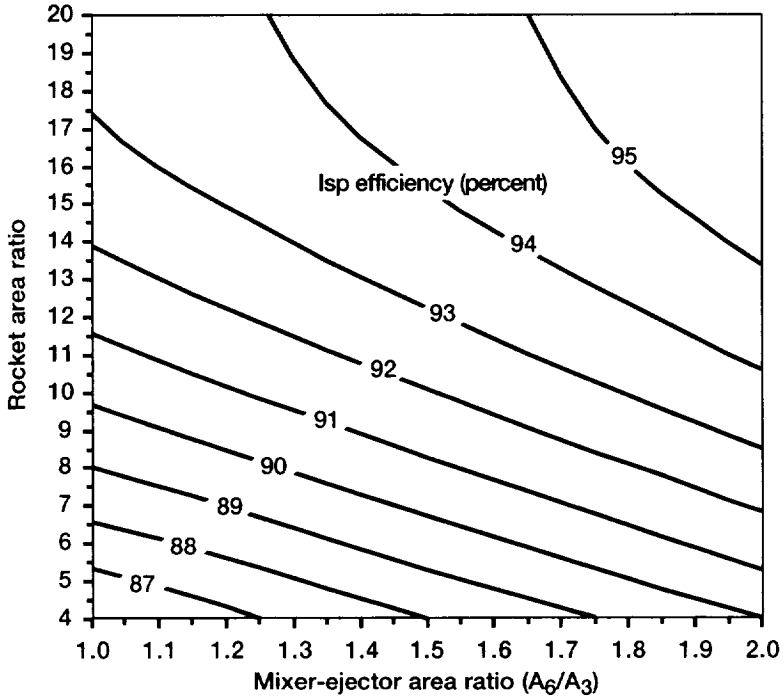

Figure 12.—Gas generator analysis-rocket area ratio as a function of mixer-ejector area ratio. (Baseline: Pc = 750 psia, m_s = 4%, A_3/A^* = 120, L/D_3 = 3.5, A_6/A_3 = 1.5, ϵ_r = 12).

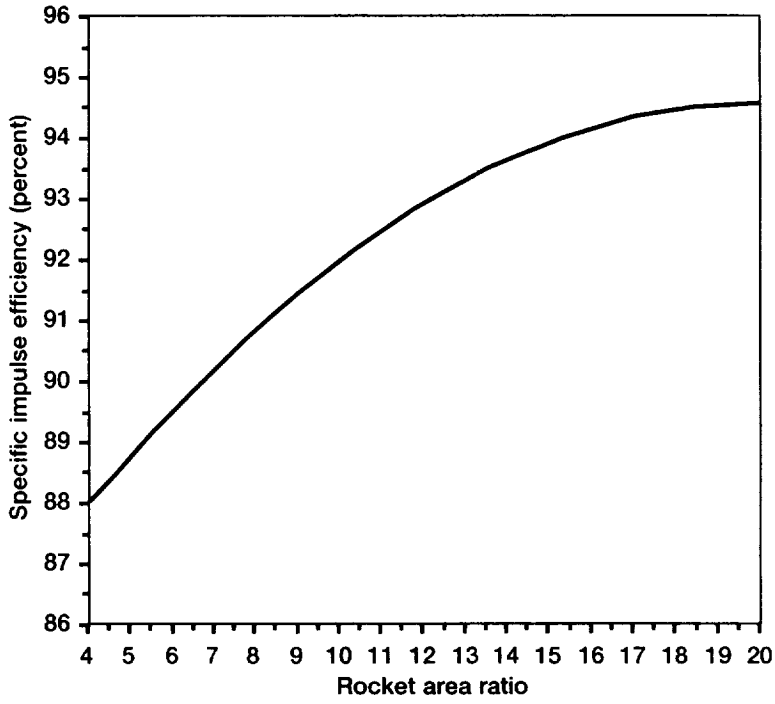

Figure 13.—Gas generator analysis-specific impulse efficiency as a function of rocket area ratio. (Baseline: Pc = 750 psia, m_s = 4%, A_3/A^* = 120, L/D_3 = 3.5, A_6/A_3 = 1.5, ϵ_r = 12).

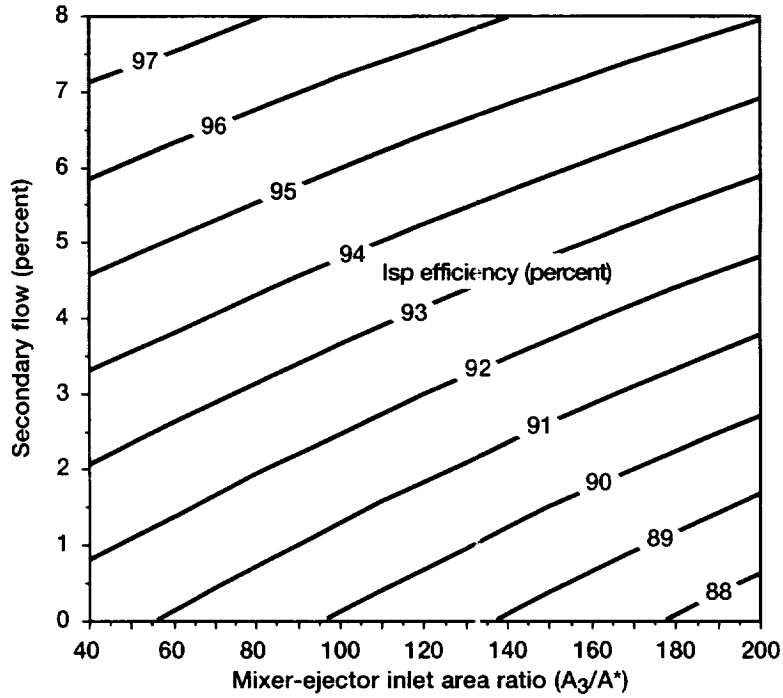

Figure 14.—Gas generator analysis-secondary flow as a function of mixer-ejector inlet area ratio. (Baseline: Pc = 750 psia, m_s = 4%, A_3/A^* = 120, L/D_3 = 3.5, A_6/A_3 = 1.5, ϵ_r = 12).

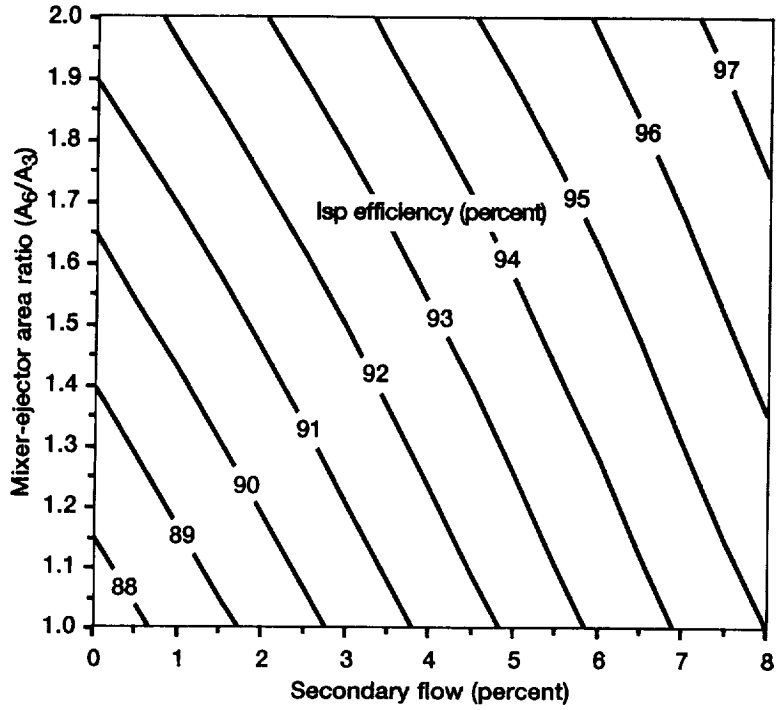

Figure 15.—Gas generator analysis-mixer-ejector area ratio as a function of secondary flow. (Baseline: Pc = 750 psia, m_s = 4%, A_3/A^* = 120, L/D_3 = 3.5, A_6/A_3 = 1.5, ϵ_r = 12).

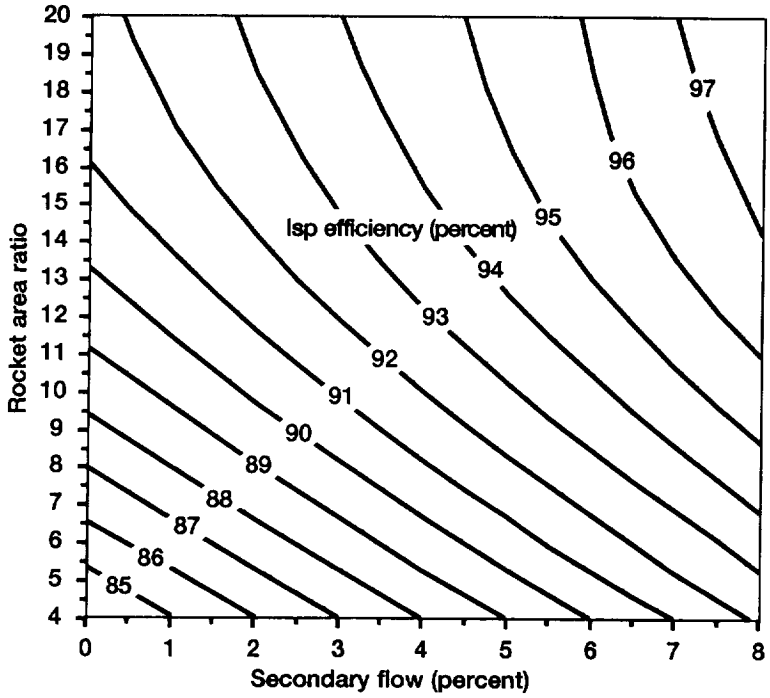

Figure 16.—Gas generator analysis-rocket area ratio as a function of secondary flow. (Baseline: Pc = 750 psia, m_s = 4%, A_3/A^* = 120, L/D_3 = 3.5, A_6/A_3 = 1.5, ϵ_r = 12).

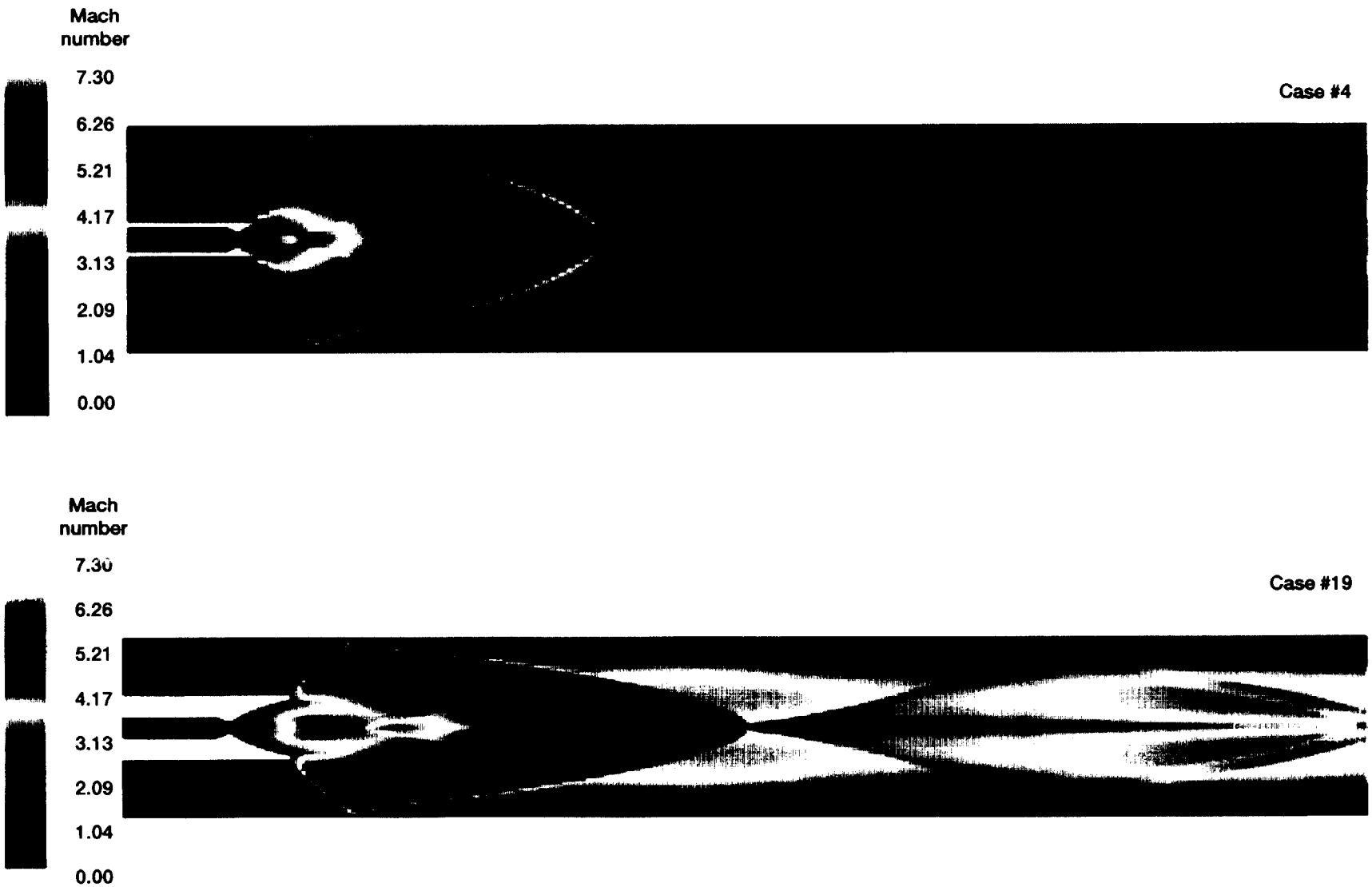

Figure 17.—Mach number contour plots comparing case #4 and case #19 showing the effect of changing rocket exit area ratio on the flowpath.

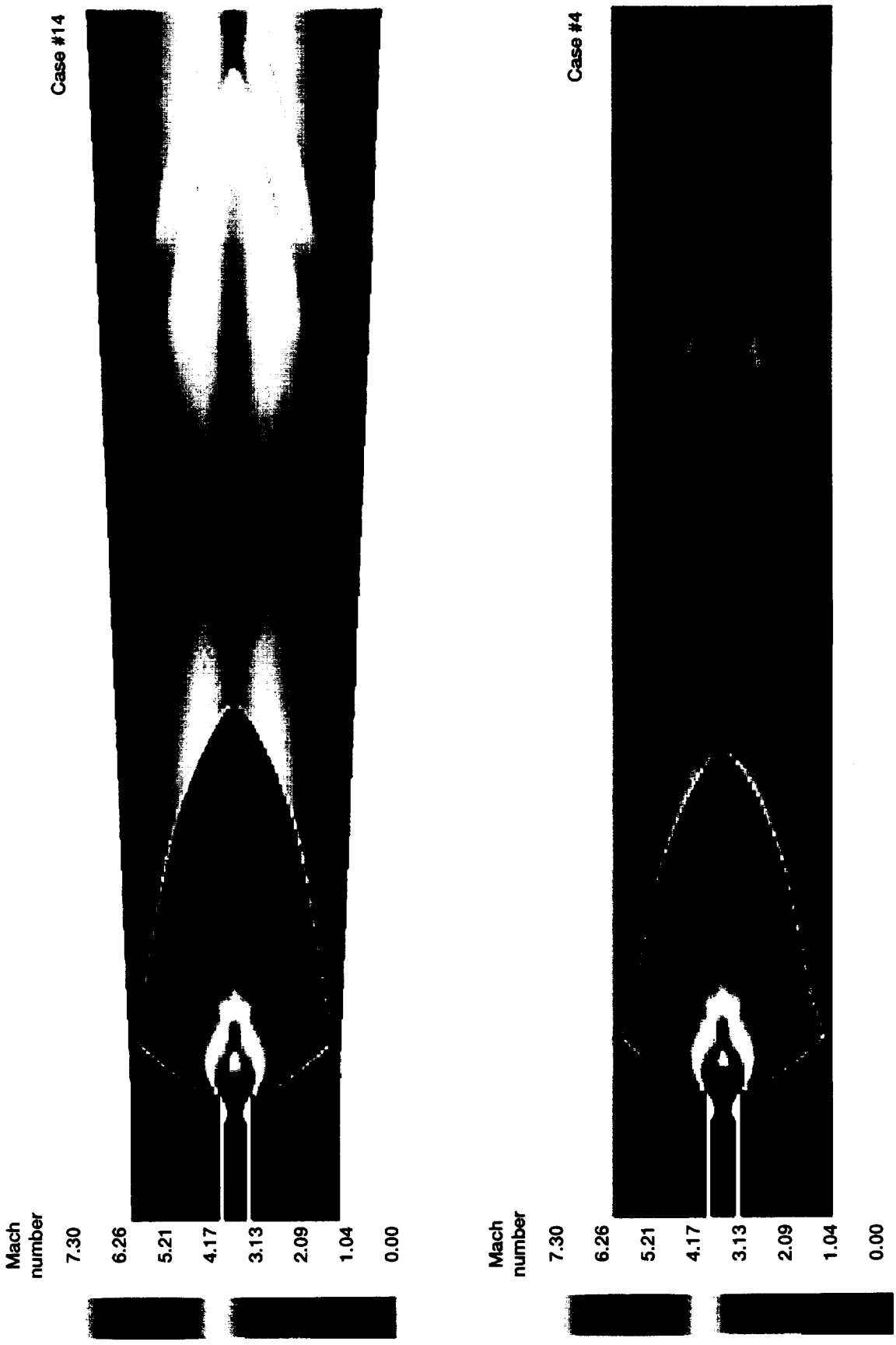

Figure 18.—Mach number contour plots comparing case #4 and case #14 showing the effect of changing mixer-ejector area ratio on the flowpath.

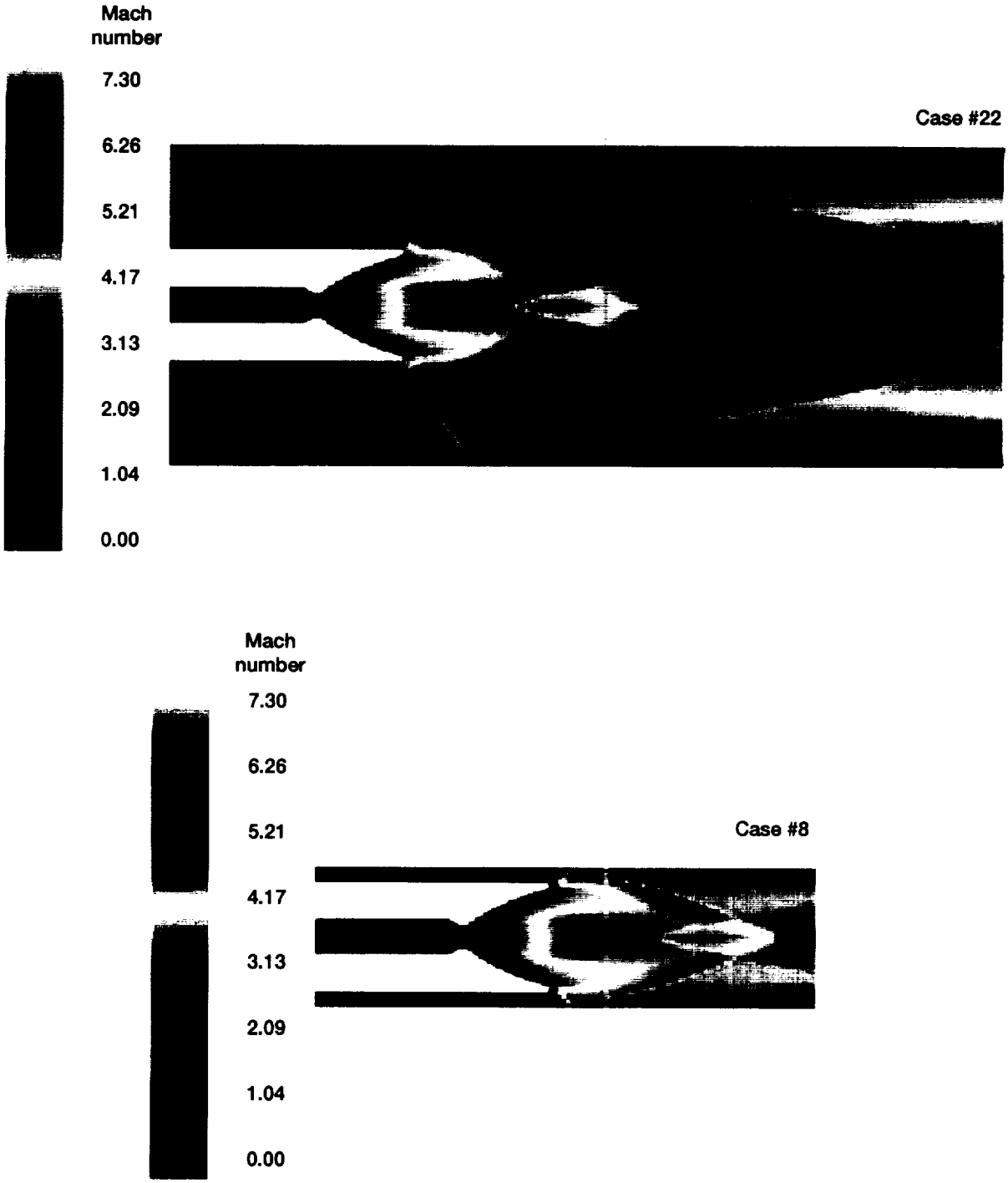

Figure 19.—Mach number contour plots comparing case #8 and case #22 showing the effect of changing mixer-ejector inlet area ratio on the flowpath.

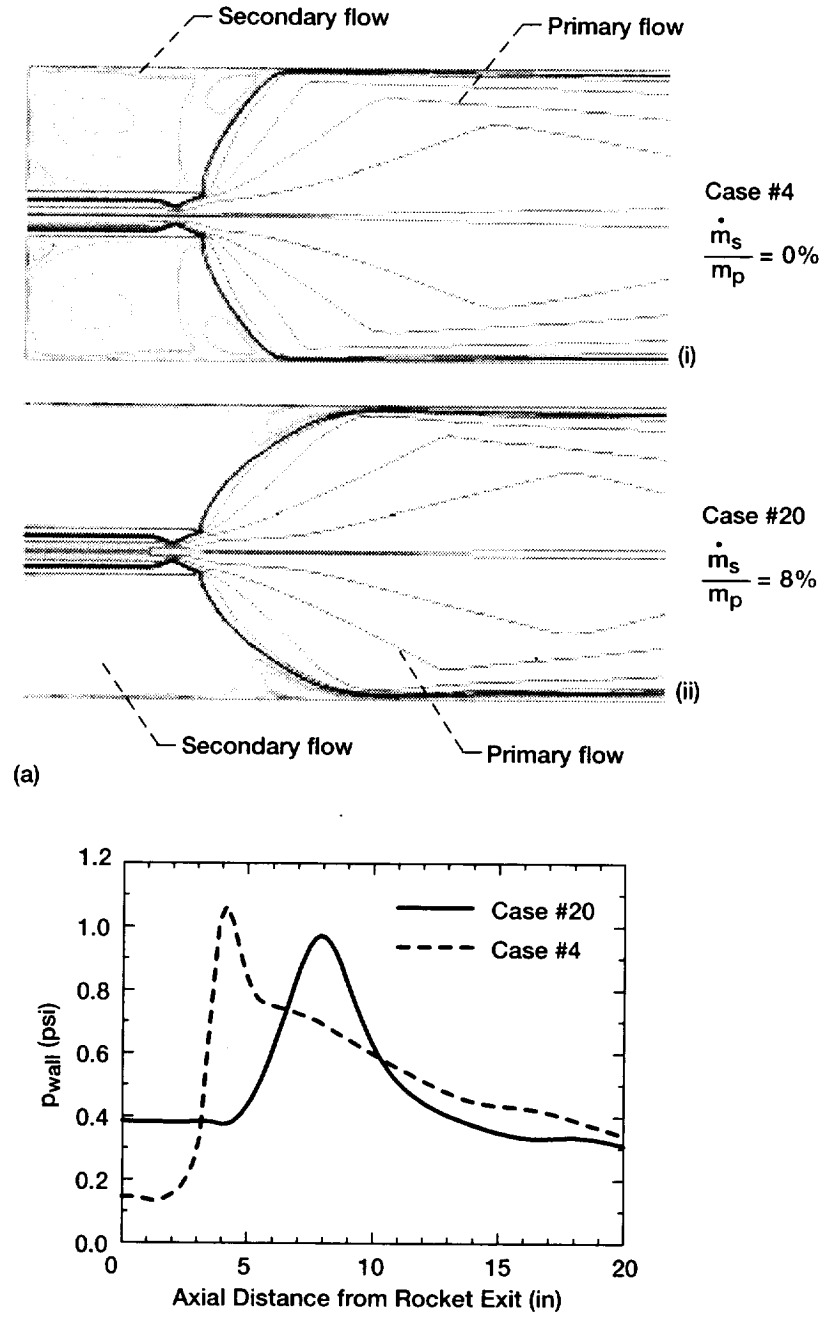

Figure 20.— (a) Particle traces; gray represents the secondary flow streaklines, black represents the primary flow streaklines for (i) no secondary flow (case #4) and (ii) 8% secondary flow (case #20). (b) Mixer-ejector surface pressure comparison; notice the effect of secondary flow upon the peak pressure (shock impingement).

REPORT DOCUMENTATION PAGE

Form Approved
OMB No. 0704-0188

1. AGENCY USE ONLY (*Leave blank*)	2. REPORT DATE	3. REPORT TYPE AND DATES COVERED
	October 1998	Technical Memorandum

4. TITLE AND SUBTITLE

Analysis of a Rocket Based Combined Cycle Engine During Rocket Only Operation

5. FUNDING NUMBERS

WU-242-72-01-00

6. AUTHOR(S)

T.D. Smith, C.J. Steffen, Jr., S. Yungster, and D.J. Keller

7. PERFORMING ORGANIZATION NAME(S) AND ADDRESS(ES)

National Aeronautics and Space Administration
Lewis Research Center
Cleveland, Ohio 44135-3191

8. PERFORMING ORGANIZATION REPORT NUMBER

E-11106

9. SPONSORING/MONITORING AGENCY NAME(S) AND ADDRESS(ES)

National Aeronautics and Space Administration
Washington, DC 20546-0001

10. SPONSORING/MONITORING AGENCY REPORT NUMBER

NASA TM—1998-206639/REV1

11. SUPPLEMENTARY NOTES

Prepared for the 1998 Propulsion Meeting sponsored by the Joint Army-Navy-NASA-Air Force, Cleveland, Ohio, July 15-17, 1998. T.D. Smith and C.J. Steffen, Jr., NASA Lewis Research Center; S. Yungster, Institute for Computational Mechanics in Propulsion, Cleveland, Ohio 44135; D.J. Keller, RealWorld Quality Systems, Inc., Cleveland, Ohio 44116. Responsible person, T.D. Smith, organization code 5830, (216) 977-7546.

12a. DISTRIBUTION/AVAILABILITY STATEMENT

Unclassified - Unlimited
Subject Category: 20 Distribution: Nonstandard

This publication is available from the NASA Center for AeroSpace Information, (301) 621-0390.

12b. DISTRIBUTION CODE

13. ABSTRACT ***(Maximum 200 words)***

The all rocket mode of operation is a critical factor in the overall performance of a rocket based combined cycle (RBCC) vehicle. However, outside of performing experiments or a full three dimensional analysis, there are no first order parametric models to estimate performance. As a result, an axisymmetric RBCC engine was used to analytically determine specific impulse efficiency values based upon both full flow and gas generator configurations. Design of experiments methodology was used to construct a test matrix and statistical regression analysis was used to build parametric models. The main parameters investigated in this study were: rocket chamber pressure, rocket exit area ratio, percent of injected secondary flow, mixer-ejector inlet area, mixer-ejector area ratio, and mixer-ejector length-to-inlet diameter ratio. A perfect gas computational fluid dynamics analysis was performed to obtain values of vacuum specific impulse. Statistical regression analysis was performed based on both full flow and gas generator engine cycles. Results were also found to be dependent upon the engine cycle assumptions. The statistical regression analysis determined that there were five significant linear effects, six interactions, and one second-order effect. Two parametric models were created to provide performance assessments of an RBCC engine in the all rocket mode of operation.

14. SUBJECT TERMS

Rocket based combined cycle; Computational fluid dynamics; Rocket nozzles; Specific impulses

15. NUMBER OF PAGES

34

16. PRICE CODE

A03

17. SECURITY CLASSIFICATION OF REPORT	18. SECURITY CLASSIFICATION OF THIS PAGE	19. SECURITY CLASSIFICATION OF ABSTRACT	20. LIMITATION OF ABSTRACT
Unclassified	Unclassified	Unclassified	